NMR Structures of the Second Transmembrane Domain of the Human Glycine Receptor α_1 Subunit: Model of Pore Architecture and Channel Gating

Pei Tang,*† Pravat K. Mandal,* and Yan Xu*†
Department of *Anesthesiology and Critical Care Medicine and †Department of Pharmacology, University of Pittsburgh School of Medicine, Pittsburgh, Pennsylvania 15261 USA

ABSTRACT Glycine receptors (GlyR) are the primary inhibitory receptors in the spinal cord and belong to a superfamily of ligand-gated ion channels (LGICs) that are extremely sensitive to low-affinity neurological agents such as general anesthetics and alcohols. The high-resolution pore architecture and the gating mechanism of this superfamily, however, remain unclear. The pore-lining second transmembrane (TM2) segments of the GlyR α_1 subunit are unique in that they form functional homopentameric channels with conductance characteristics nearly identical to those of an authentic receptor (Opella, S. J., J. Gesell, A. R. Valente, F. M. Marassi, M. Oblatt-Montal, W. Sun, A. F. Montiel, and M. Montal. 1997. *Chemtracts Biochem. Mol. Biol.* 10:153–174). Using NMR and circular dichroism (CD), we determined the high-resolution structures of the TM2 segment of human α_1 GlyR and an anesthetic-insensitive mutant (S267Y) in dodecyl phosphocholine (DPC) and sodium dodecyl sulfate (SDS) micelles. The NMR structures showed right-handed α-helices without kinks. A well-defined hydrophilic path, composed of side chains of G2′, T6′, T10′, Q14′, and S18′, runs along the helical surfaces at an angle ~10-20° relative to the long axis of the helices. The side-chain arrangement of the NMR-derived structures and the energy minimization of a homopentameric TM2 channel in a fully hydrated DMPC membrane using large-scale computation suggest a model of pore architecture in which simultaneous tilting movements of entire TM2 helices by a mere 10° may be sufficient to account for the channel gating. The model also suggests that additional residues accessible from within the pore include L3′, T7′, T13′, and G17′. A similar pore architecture and gating mechanism may apply to other channels in the same superfamily, including $GABA_A$, nACh, and 5-HT_3 receptors.

INTRODUCTION

The pore architecture and the gating mechanism of a superfamily of neurotransmitter-gated ion channels, including glycine, γ-aminobutyric acid type A ($GABA_A$), nicotinic acetylcholine (nACh), and serotonin 5-HT_3 receptors remain poorly understood. This superfamily is responsible for the fast synaptic transmission in the central nervous system and has been shown to be particularly sensitive to low-affinity neurological agents such as volatile general anesthetics and short-chain alcohols (Franks and Lieb, 1996). Although the crystal structure of an acetylcholine-binding protein, which resembles the extracellular domain of nAChR, has recently been resolved (Brejc et al., 2001), the high-resolution structural information of the transmembrane domains of this superfamily is generally lacking. The pore-lining elements and their role in channel activation and gating are mostly inferred from the substituted-cysteine accessibility measurements (Karlin and Akabas, 1998) or from electron microscopy at a 9-Å resolution (Unwin, 1998).

In general, the membrane-associated ligand-gated ion channels (LGICs) in their intact forms are refractory to experimental high-resolution structural determinations. To obtain structural information with atomic resolution, an alternative approach has recently been proposed to delineate the crucial architecture of the transmembrane pore by recapitulating the active moiety and studying the functional segments of the putative pore-lining second transmembrane (TM2) domains in a membranous environment (Opella et al., 1999). The GlyR is particularly suited for this approach because the TM2 segments of the human α_1 subunit alone form homopentameric channels with conductance characteristics nearly identical to those of an authentic receptor (Marsh, 1996; Opella et al., 1997; Reddy et al., 1993). Recent experimental evidence from a different transmembrane protein (Kochendoerfer et al., 1999; Salom et al., 2000) further demonstrates that solubilizing small functional transmembrane segments in dodecylphosphocholine (DPC) can form correct channel bundles, suggesting that the DPC micelles provide an adequate membrane-mimicking environment for correct transmembrane protein aggregation and folding.

Using the same approach, we determined the structure of the TM2 domain of the human GlyR α_1 subunit in DPC and sodium dodecyl sulfate (SDS) micelles. In addition, we also determined the TM2 structure of a unique single-point mutant, S267Y. This mutant and its analog in $GABA_A$ receptors are found to have distinctly different sensitivity to low-affinity but receptor-specific neurological agents, such as volatile anesthetics and alcohols (Mihic et al., 1997). Based on the NMR-derived monomer TM2 structures, we

Submitted November 14, 2001 and accepted for publication March 7, 2002.
Address reprint requests to Prof. Yan Xu, W-1358 Biomedical Science Tower, University of Pittsburgh School of Medicine, Pittsburgh, PA 15261. Tel.: 412-648-9922; Fax: 412-648-9587; E-mail: xuy@anes.upmc.edu.

0006-3495/02/07/252/11 $2.00

further determined the plausible pore architecture by extensive energy minimization of homopentameric GlyR α_1 TM2 channels in a fully hydrated 1,2-dimyristoyl-*sn*-glycero-3-phosphocholine (DMPC) membrane (Zubrzycki et al. 2000) by using a large-scale computer simulation. The NMR-derived structures and computation-based homopentameric pore architecture revealed a sufficient amount of atomic details that are potentially relevant to channel gating.

EXPERIMENTAL PROCEDURES

Sample preparation

The wild-type TM2 segment ($TM2_{WT}$) of the human GlyR α_1 subunit has a sequence (Grenningloh et al., 1990) of PARVGLGITTVLTMTTQSSG-SRA, in which the two arginines (R252 and R271) are numbered as R0′ and R19′, respectively, using the convention suggested by Miller (1989). For $TM2_{S267Y}$, the underlined S15′ is replaced by Y. In this study, both $TM2_{WT}$ and $TM2_{S267Y}$ were synthesized by solid-phase synthesis and purified by reverse-phase HPLC. A special procedure, modified from that described by Killian et al. (1994) was used to incorporate the peptides into the DPC or SDS micelles so that the samples were stable for prolonged NMR data acquisition. Briefly, the purified peptides were first dissolved in trifluoroacetic acid and then dried into a thin film under a stream of N_2 gas. Thereafter, 2,2,2-trifluoroethanol (TFE) was added to prepare a TM2 solution of 25 m*M*. Separately, a 1000-m*M* solution of deuterated DPC or SDS micelles in H_2O was prepared. Aliquots of the peptide solution were titrated to the micelle solution to reach a peptide-to-micelle molar ratio of 1:220. Water was then added to yield a water-to-TFE ratio of 16:1 by volume. The samples were mixed vigorously for 5 s, rapidly frozen in solid CO_2/acetone, and lyophilized overnight at −50°C. The lyophilized samples were further vacuumed for at least 24 h to ensure nearly complete removal of the organic solvents and then rehydrated with deionized water (90% H_2O and 10% D_2O). A typical NMR sample contained 3.1 m*M* peptides in 677 m*M* DPC or SDS, with pH adjusted to 4.8. For circular dichroism (CD) experiments, aliquots of NMR samples were diluted by a factor of ~52 to reach a peptide concentration of 60 μM and then used.

SDS-polyacrylamide gel electrophoresis (SDS-PAGE)

The oligomerization state of TM2 segments in micelles was determined using the SDS-PAGE, as described by Tatulian and Tamm (2000). Gradient gels of 12% and 20% acrylamide solution were used, containing *N*,*N*′-methylenebisacrylamide at an acrylamide bisacrylamide molar ratio of 30:1 in an aqueous buffer of 0.1% SDS, 5% glycerol, 0.06 mM EDTA, 0.3 M glycine, and 0.1 M Tris HCl (pH 8.8). Peptide samples for electrophoresis were prepared using the same procedure as for NMR samples, except that the final resuspension was in an aqueous buffer solution (0.1 M NaCl and 10 mM Hepes at pH 7.2), followed by the addition of the treatment buffer (0.125 M Tris-HCl, 4% SDS, 20% glycerol, 10% β-mercaptoethanol, pH 6.8) in a 1:1 volume ratio. The electrophoresis was conducted at 20 mA constant current for 1 h using a buffer of 25 mM Tris, 192 mM glycine, 0.1% SDS, and pH 8.3. The gels were stained for 30 min using 0.1% Coomassie Blue R-250.

CD spectroscopy

CD experiments were carried out on a Jasco-710 spectropolarimeter. All measurements were made at 30°C in a quartz cuvette of 1-mm path length. Spectra were recorded over the far-UV range of 180-260 nm with a time constant of 1 s, a spectral resolution of 1 nm, and a scan rate of 20 nm/min. Three scans were averaged for each spectrum, and the reference spectra of the respective media were subtracted. The fraction of residues in the α-helical conformation, f_H, was estimated from the measured residue ellipticity at 222 nm, θ_{222}, using the well-established method (Luo and Baldwin, 1997; Tatulian and Tamm, 2000): $f_H = (\theta_{222} - \theta_C)/(\theta_H - \theta_C)$, where the temperature-dependent values for an infinite helix, θ_H and a random coil, θ_C, are assumed to be −31739 and −3400 deg/cm^2/dmol^{-1}, respectively (Luo and Baldwin, 1997; Scholtz et al., 1995).

NMR spectroscopy

The NMR experiments were conducted at 30°C on Bruker DMX750 and DMX600 spectrometers equipped with inverse-detection probes. Two-dimensional ^{1}H-TOCSY and NOESY spectra were acquired in 4096 × 512 complex points using WATERGATE (Piotto et al., 1992) for water suppression and the States-TPPI (Marion and Wuthrich, 1983) for quadrature detection in the t_1 dimension. The NOESY mixing time was 100 ms and the TOCSY MLEV17 spin-lock time was 51.8 and 81.4 ms. The spectra were processed using the NMRPipe program (Delaglio et al., 1995) and analyzed with the PIPP program (Garrett et al., 1991). For structural calculation, distance restraints were grouped into three categories, 2.0–2.8 Å, 2.0–3.5 Å, and 2.0–4.5 Å, for strong, medium, and weak NOEs. The initial structure calculations were done using only the NOE constraints with the standard three-stage distance geometry and simulated annealing protocol (Nilges et al., 1988), using X-PLOR version 3.851 (Brünger, 1992). Those with no violations above the threshold conditions of 5° for angle, improper, and dihedral angles, and 0.05 Å and 0.5 Å for bonds and NOEs, respectively, were taken for further analysis. In reference to the CD data of α-helical contents (see below), which were confirmed by the initial structural calculation, we also included in the further calculation and refinement hydrogen bond constraints of CO(i) to NH(i + 4) for those residues where $d_{\alpha N}(i,i+3)$ and $d_{\alpha\beta}(i,i+3)$ NOE connectivity is present. Each hydrogen bond was converted into two distance restraints $r_{NH\text{-}O}$ (1.8–2.2 Å) and $r_{N\text{-}O}$ (2.2–3.3 Å) (Opella et al., 1999; Tochio et al., 1998). The 30 lowest-energy structures were used for refinement by including the dihedral terms and the standard Lennard-Jones function for electrostatic interactions. The VMD program (Humphrey et al., 1996) was used for structural rendering.

Large-scale, all-atom energy minimization

To study possible pore architecture, the NMR-derived structures were used to construct a homopentameric TM2 channel based on the 9-Å resolution crystallography data, which suggest a pseudo-fivefold symmetry for this superfamily of ion channels. The homopentameric channels were subjected to extensive energy minimization in a preequilibrated DMPC membrane (Zubrzycki et al., 2000). The channel, membrane, and a cylinder of TIP3 waters (Jorgensen et al., 1983) through the pore were superimposed and all lipid and water molecules that were within van der Waals contact with any atoms of the channel were deleted, resulting in 159 lipids and 5674 waters in the final system. Energy minimization was performed on the T3E supercomputer at the Pittsburgh Supercomputing Center using the NAMD2 program (Nelson et al., 1996) with the CHARMM-22 force field for proteins and lipids (MacKerell et al., 1998; Schlenkrich et al., 1996). The particle-mesh Ewald method was used to take into account full electrostatic interactions with the periodical boundary condition in a flexible cell of 90 × 90 × 70 Å^3. The conjugate gradient and line search algorithm (Polak 1971) was used for energy minimization in two stages. The first stage was done without counterions until the relative energy change was $<10^{-3}$, at which point 10 randomly selected water molecules were replaced by 10 Cl^- ions. The second stage continued until the relative change in total energy was $<10^{-5}$. The Hole program (Smart et al., 1996) was used to determine the radius profiles of the channels.

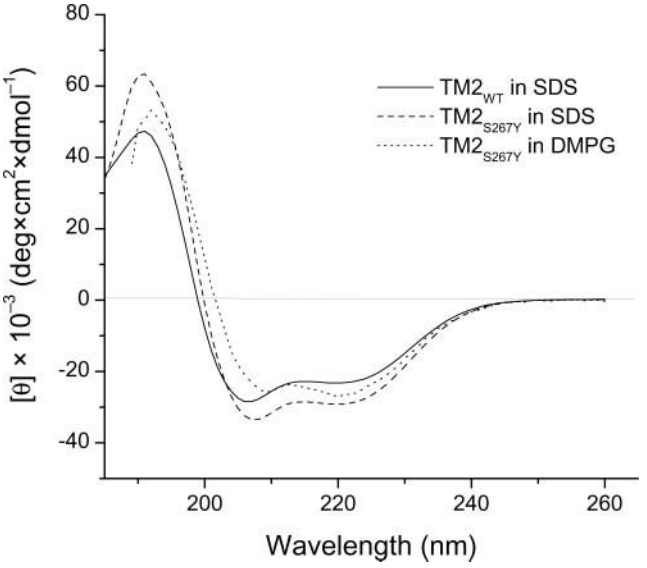

FIGURE 1 CD spectra of the functional segments of the pore-lining second transmembrane domain ($TM2_{WT}$) of human glycine receptor α_1 subunits in SDS micelles (*solid line*) and the anesthetic-insensitive $TM2_{S267Y}$ mutant in SDS micelles (*dashed line*), and in DMPG lipid bilayers (*dotted line*). Spectra of the same peptides in DPC are very similar. The fraction of α-helical conformation for $TM2_{WT}$ and $TM2_{S267Y}$ in micelles can be estimated based on the mean residue molar ellipticity at 222 nm to be 70% and 91%, respectively. All spectra were averages of three scans recorded at 30°C after subtraction of the reference spectra of the media.

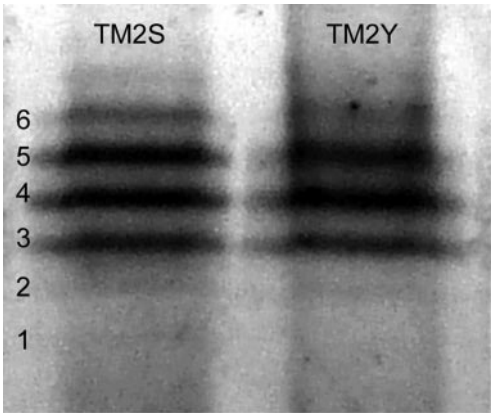

FIGURE 2 SDS-PAGE gel showing the coexistence of multiple oligomeric states of GlyR TM2 segments in DPC micelles. The lowest band, which is very faint but positively identified by the gel analysis program, is assumed to be the monomers encapsulated in DPC micelles. The weight differences between adjacent bands are in excellent agreement with the molecular weight of a single TM2 segment.

RESULTS

Structural description

In DPC and SDS micelles we found that both $TM2_{WT}$ and $TM2_{S267Y}$ had stable α-helical structures. CD spectral analysis of highly purified GlyR $TM2_{WT}$ and $TM2_{S267Y}$ segments in SDS (Fig. 1) yielded an estimate of 70% and 91% α-helical components, respectively. Similar CD spectra were also obtained in DPC. Because TM2 segments are known to form functional pentameric channels with conductance properties nearly identical to those of an authentic receptor (Marsh, 1996; Opella et al., 1997; Reddy et al., 1993), we also carried out CD experiments on TM2 segments incorporated into 1,2-dimyristoyl-*sn*-glycero-3-phosphoglycerol vesicles. The CD spectrum in vesicles (Fig. 1) shows that TM2 in the lipid bilayers is also predominantly α-helical, confirming that the TM2 conformation in SDS and DPC micelles mimics that in lipid bilayers, and thus validating the reductionist approach to the structural determination of transmembrane segments in SDS or DPC micelles. The oligomerization states of TM2 in DPC micelles were determined using SDS-PAGE, as shown in Fig. 2. Using the Kodak 1_D gel analysis program we positively identified seven bands, of which trimers, tetramers, and pentamers are predominant. Contrary to common belief, monomers are not the most popular state of TM2 in micelles. In fact, monomers of $TM2_{S267Y}$ are hardly visible in the gel. This is understandable because the TM2 helix, as the channel lining segment, has distinct hydrophilic and hydrophobic surfaces along the helix (see below). Hydrophobic interaction with micelle interior disfavors the monomer or even dimer formation. Higher (>8) orders of oligomerization states, if any, are too low in concentration to be detected by the gel. The 750-MHz and 600-MHz ^{1}H-NMR spectra of $TM2_{WT}$ and $TM2_{S267Y}$ segments in deuterated DPC and SDS micelles are well resolved (Fig. 3), allowing for complete sequence-specific spectral assignment (Tang et al., 1999c) and structural determination. All peaks in the backbone amide and α proton region and most of the side chain protons were unambiguously assigned. In all, there are 184, 175, 193, and 187 NOE crosspeaks for $TM2_{WT}$ in DPC and SDS and mutant $TM2_{S267Y}$ in DPC and SDS, respectively. The chemical shift differences between $TM2_{WT}$ and $TM2_{S267Y}$ are generally small except for residues near the point of mutation, suggesting that mutation affects the local conformation without drastically changing the overall secondary structure of the channel pore. The sequential and mid-range NOE connectivity, as summarized in Fig. 4, *A* and *B*, extends throughout the entire sequence of $TM2_{WT}$ and $TM2_{S267Y}$. In particular, the αN and $\alpha\beta$ NOE connectivity of three residues apart, a characteristic of α-helical structure, extends from V1′ to S16′ in $TM2_{WT}$ and from V1′ to S18′ in $TM2_{S267Y}$. Although TM2 segments are present in multiple oligomeric states in micelles (see Fig. 2), no intersegment NOE cross peaks from neighboring side chains were detectable, presumably due to rapid motions of the segments relative to each other. Thus, while different oligomeric states coexist in micellar preparations, the fact that only a single set of NOE connectivity exists and that NMR peaks are relatively narrow suggests that the TM2

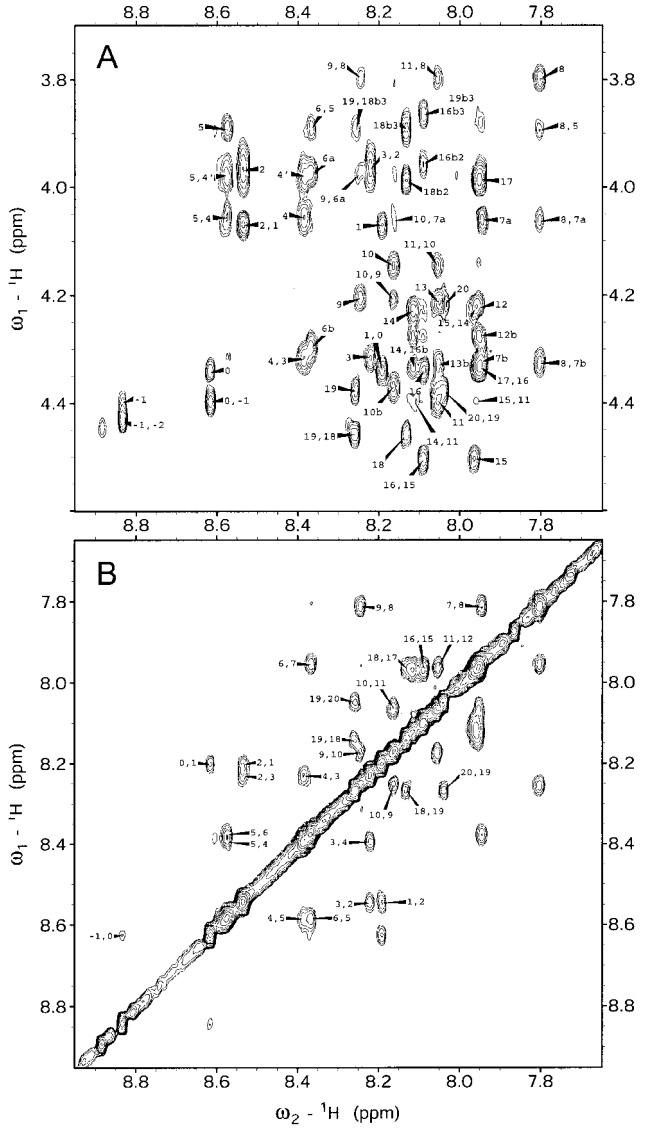

FIGURE 3 Representative 750-MHz ^{1}H-NOESY spectrum of GlyR TM2 in DPC micelles, showing (*A*) the H_N-H_α (fingerprint), and (*B*) the H_N-H_N regions. The exceptional resolution at high magnetic field allows for complete sequence-specific assignments and structural determination. All assigned peaks are labeled using the relative numbering system of the peptide sequence and following the ω_2, ω_1 convention.

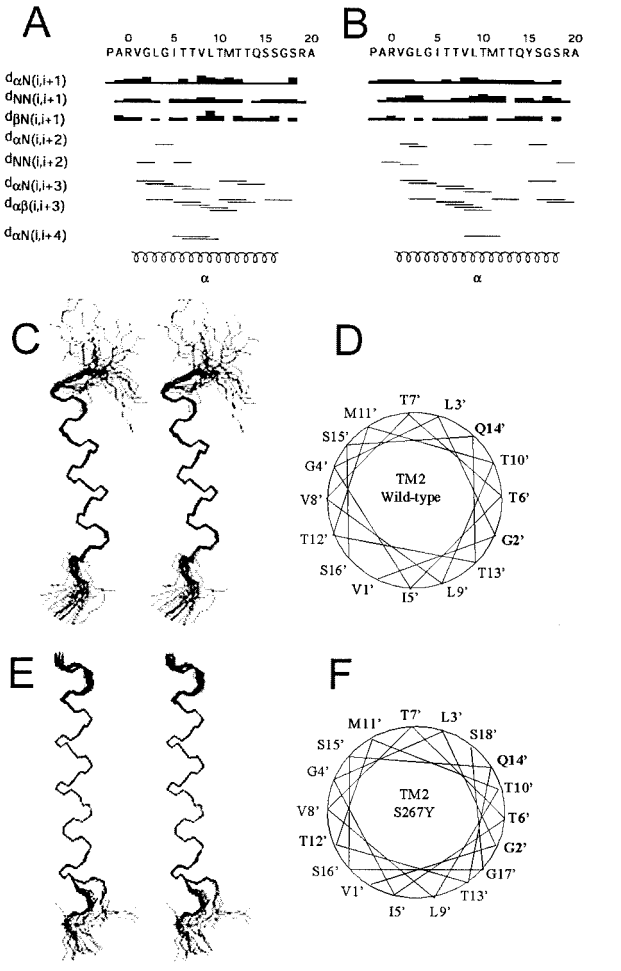

FIGURE 4 NMR determination of the TM2 structures of human glycine receptor. Sequential and mid-range NOE connectivity is plotted for the functional α_1 GlyR $TM2_{WT}$ (*A*) and its anesthetic-insensitive $TM2_{S267Y}$ mutant (*B*). Lines indicate that the NOEs were unambiguously identified and assigned; the widths of the lines are related to the observed NOE intensities. An α-helical pattern can be identified from V1′ to S16′ in $TM2_{WT}$ and from V1′ to S18′ in $TM2_{S267Y}$. The first 30 lowest energy structures (stereo view, C-terminals at top) are depicted for $TM2_{WT}$ (*C*) and $TM2_{S267Y}$ (*E*) in SDS micelles. Structures in DPC are very similar. The corresponding helical wheels (*D* and *F*) revealed a well-defined hydrophilic face along the helix, composed of G2′, L3′, T6′, T7′, T10′, Q14′, G17′, and S18′, which either line or border the channel pore.

structures do not differ significantly among different oligomeric states, and that the structures determined by the NMR are common to all oligomeric states. Fig. 4 *C* and *E* shows stereo views of 30 structures for $TM2_{WT}$ and the $TM2_{S267Y}$ in SDS, respectively. The statistics for these structures, which have no NOE violation >0.5 Å and dihedral angle violation $>5°$, are given in Table 1.

The NMR-derived structures of $TM2_{WT}$ and $TM2_{S267Y}$ segments in the membrane-mimicking environment have well-defined hydrophilic and hydrophobic faces along the cylindrical surface of the helices, as shown in Fig. 4 *D* and *F*. These surfaces are depicted in Fig. 5 using a color hydrophobicity scale (Kyte and Doolittle, 1982). The continuous hydrophilic surface, composed of G2′, T6′, T10′, Q14′, and S18′, is likely to be part of the pore lining of the open channel. Notice that this hydrophilic surface, not interrupted by hydrophobic residues, runs at a tilted angle ($\sim$10–20°) relative to the long axis of the helices. To consider possible ways of arranging the high-resolution NMR-derived GlyR TM2 structures into a pentameric pore, a rational assumption is that the tilted hydrophilic surface faces the center of the channel (the tilted solid line in Fig. 5). In this configuration, there are at least three extruding points composed of the side chains of T6′, T10′, and Q14′,

TABLE 1 Statistics for families of 30 human GlyR $TM2_{WT}$ and $TM2_{S267Y}$ structures

Property	WT (DPC)	WT (SDS)	S267Y (DPC)	S267Y (SDS)
Distance Restraints				
Intraresidue ($\|i-j\|=0$)	105	112	120	107
Sequential ($\|i-j\|=1$)	59	37	51	53
Medium range ($2 \le \|i-j\| \le 4$)	20	26	22	27
Number of NOEs per residues	8.0	7.6	8.4	8.1
Number of H-bond restraints (2 per bond)	22	24	24	26
Total number of restraints	206	199	217	213
Number of refined structures	30	30	30	30
Energy (kcal/mol)				
E^*_{NOE}	56.06 ± 3.03	69.27 ± 5.76	73.45 ± 4.72	78.01 ± 2.36
E^*_{dihe}	24.76 ± 3.36	29.94 ± 5.48	57.73 ± 5.61	55.1 ± 4.39
E_{lmpr}	14.64 ± 0.70	6.55 ± 0.65	9.58 ± 0.77	8.33 ± 0.70
E_{Ele}	−185.2 ± 14.9	−217.4 ± 17.2	−212.9 ± 14.1	−208.2 ± 17.3
Atomic r.m.s.d (Å)†				
Backbone (helical region)	0.10 ± 0.02	0.19 ± 0.06	0.17 ± 0.06	0.22 ± 0.14
All heavy atoms	2.38 ± 0.87	2.14 ± 0.33	2.10 ± 0.31	1.10 ± 0.36
Ramachandran analysis‡				
% residues in				
favored region	91.31%	78.3%	95.96%	87.62%
additional allowed region	8.69%	21.7%	4.34%	4.34%
generously allowed region	0%	0%	0%	8.60%
disallowed region	0%	0%	0%	0%

None of the structures has distance violations >0.5 Å and dihedral angle violations >5°.
*The final values of square-well NOE and dihedral-angle potentials were calculated with force constants of 50 kcal mol^{-1} $Å^{-2}$ and 200 kcal mol^{-1} rad^{-2}.
†The r.m.s. differences were determined between the 30 final structures and the corresponding mean coordinates of the peptides after superposition of 30 structures by the backbone heavy atoms in the following range: 1′–14′ for WT (DPC), 1′–16′ for WT (SDS), 1′–16′ for S267Y (DPC), and 1′–18′ for S267Y (SDS).
‡The overall quality of the structures was evaluated by the program PROCHECK (Laskowski et al., 1996).

which form three levels of aligned "polar rings" when five subunits aggregate into a channel. These polar rings may be important for ion conductance, as discussed below.

An alternative arrangement is to align the helical cylinders along their long axes and impose a five-fold symmetry on the pore architecture. This arrangement places L3′, T6′, T7′, T10′, T13′, and G17′ within the channel lumen, with part of the hydrophobic side chain of L3′ situated at the intracellular vestibule. Most of the side chains in this arrangement are not aligned (pathways along the vertical lines in Fig. 5). Nevertheless, both docking arrangements are in good agreement with the results from the substituted-cysteine accessibility measurements, which identified within the same superfamily V2′, T6′, T7′, L9′, T10′, T13′, I16′, S17′, and N20′ in the $GABA_A$ channel and T2′, L3′, S6′, L8′, L9′, S10′, V13′, L16′, and E20′ in the nAChR channel to be accessible from the aqueous phase (Karlin and Akabas, 1998; Xu and Akabas, 1996; Xu et al., 1995).

Channel pore architecture

To further consider the atomic details and the side-chain packing of a GlyR channel pore, we immersed the homopentameric $TM2_{WT}$ and $TM2_{S267Y}$ channels in a fully hydrated DMPC membrane and performed large-scale, all-atom energy minimization in the presence of 10 Cl^- counterions. The NMR-derived $TM2_{WT}$ and $TM2_{S267Y}$ structures were docked into homopentameric channels with the T6′ side-chain vector (linear least-squares fit through the coordinates of Cα, Cβ, Cγ, and Oγ in the NMR structure) pointing to the center axis of the pore and being perpendicular to both the long axis of the monomer helical axis and the pore axis. For a tilted arrangement, the same T6′ side-chain vector was used for a 10° tilting rotation of the helix. Five copies of the monomer were generated with 0, 72°, 144°, 216°, and 288° rotations along the pore axis before radial displacements of 9.7 Å were made. These radial displacements of five monomers resulted in a homopentameric channel having a narrowest pore diameter of 5.0 Å and 4.9 Å in the wild-type and S267Y channel, respectively. These initial diameters were estimated from conductance measurements of various anions (Rajendra et al., 1997). The energy minimization proceeded until the relative change in total energy became $<10^{-5}$. We found that the final energy differences between the corresponding untilted and tilted configurations are very small, amounting to only 0.06% of the total energy. For both $TM2_{WT}$ and $TM2_{S267Y}$ channels, the untilted configurations are slightly energy-favored in the DMPC membrane. Fig. 6 depicts the final pore architectures of $TM2_{WT}$ after extensive energy minimization in a fully hydrated DMPC membrane. For clarity, water, lipid, and Cl^- were removed from the display. After energy minimization, while the monomer structure remained very similar to the NMR structure, the untilted configuration finished

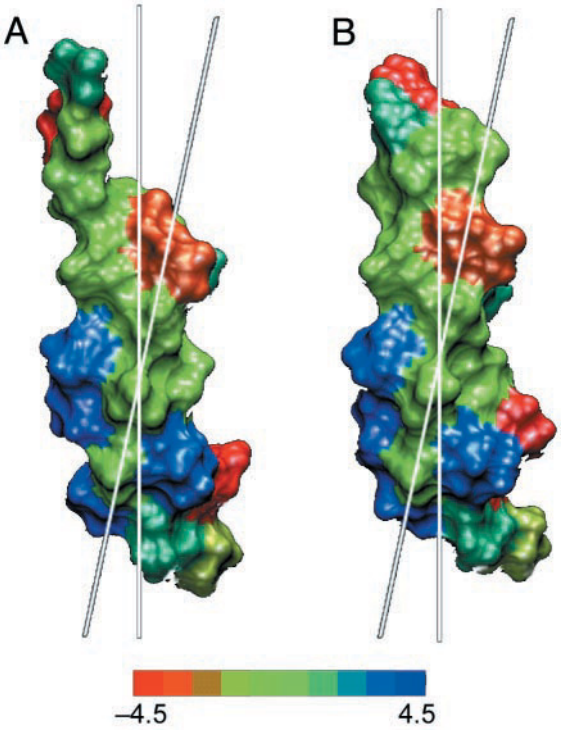

FIGURE 5 The surfaces of the human α_1 GlyR $TM2_{WT}$ (*A*) and $TM2_{S267Y}$ (*B*) helices (C-terminals at top) are graphed using an amino acid hydrophobic color scale ranging from −4.5 (most hydrophilic) to +4.5 (most hydrophobic). Notice that the continuous hydrophilic surface is running at a 10–20° angle relative to the long axis of the helices. This surface, containing four extruding hydrophilic side chains (from bottom to top along the tilted lines: G2′, T6′, T10′, and Q14′) to form potential ion-binding rings, is likely to line the pore of an open channel. A straight (untilted) arrangement of helices not only reduces the number of potential ion-binding rings, but also partially brings the large hydrophobic side chain of L3′ into the intracellular vestibule.

with a pore radius significantly smaller than in the tilted configuration. This is true for both $TM2_{WT}$ and $TM2_{S267Y}$. Fig. 7 depicts the pore radius profiles along the channel axis. The untilted configurations (*solid lines*) of both $TM2_{WT}$ and $TM2_{S267Y}$ show two constricting points at levels of T6′, and Q14′, whereas the tilted configurations (*dashed lines*) exhibit three layers of rings at T6′, T10′, and Q14′. Changing from tilted to untilted configurations, the pore diameter narrows by 1.56 Å at the level of Q14′.

DISCUSSION

We have determined the structure of the second transmembrane domain of the GlyR α_1 subunit, one of the primary subunits of the anion-selective channels in the adult spinal cord. The α-helical structure without kinks is in agreement with the NMR finding of another TM2 segment, that of the nACh receptor δ subunit (Opella et al., 1999), which belongs to the same superfamily of neurotransmitter-gated receptors but forms cation channels. Moreover, we have

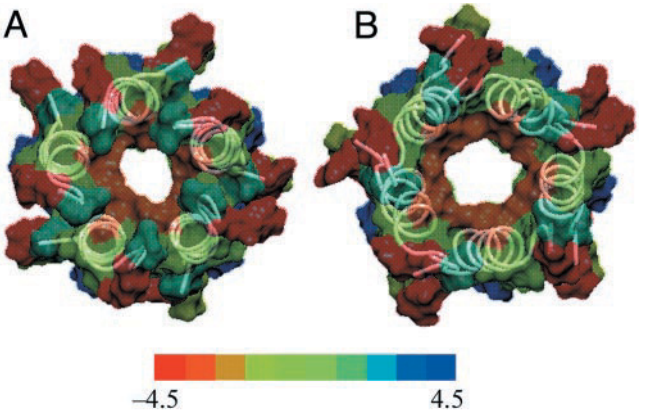

FIGURE 6 Homopentameric TM2 pore architectures (C-terminal views) of human α_1 GlyR after extensive energy minimization in a fully hydrated DMPC membrane: (*A*) the helical axes are parallel to the pore axis, and (*B*) helical axes are tilted by 10° relative to the pore axis. Notice the difference in pore diameter. The residues are colored in the same hydrophobic scale as in Fig. 4. The hydrophilic orange rings in the pore are composed of side chains of Q14′, which might play an important role in channel gating (see Discussion). *Online supplementary information:* An animation is provided to offer a pictorial view of NMR-derived pore architecture (C-terminal views, after extensive energy minimization in a fully hydrated DMPC membrane) and the proposed gating model by the entire TM2 tilting movement. The side chains of Q266 form the top orange ring within the pore.

shown with CD (Fig. 1) that the TM2 conformation in SDS or DPC micelles mimics that in DMPG lipid bilayers, in which TM2 segments of GlyR α_1 subunits are known to

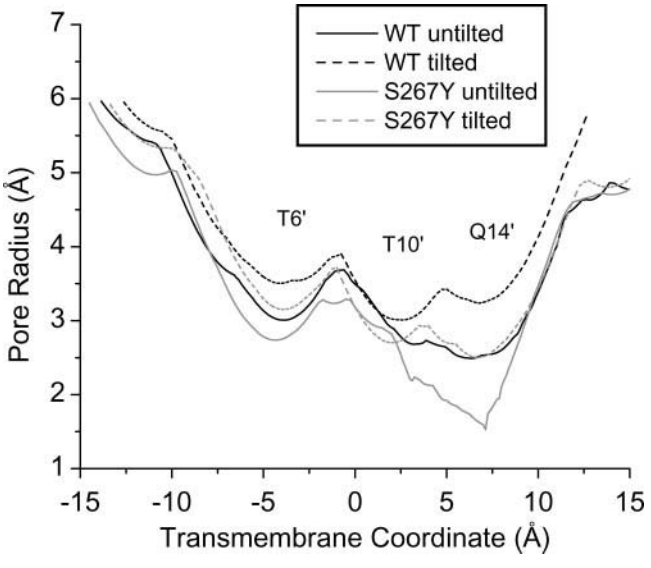

FIGURE 7 The radius profiles of homopentameric TM2 channels after extensive energy minimization in DMPC membrane. Notice the dramatic radial changes at the level of Q14′ from the untilted to the tilted configuration. Simultaneous tilting of the TM2 segments results in at least three layers of aligned hydrophilic narrowing along the channel at T6′, T10′, and Q14′. The polar hydroxyl groups of T6′ and T10′ and the amino group of Q14′ can liberate ions from their hydration shells, mediating ion transport across the channel.

form functional channels (Marsh, 1996; Opella et al., 1997; Reddy et al., 1993). Although solubilizing membrane proteins in membrane-mimetic micelles for high-resolution structural determination by NMR is a well-accepted method, its validity has only been confirmed recently by studying the oligomerization states with SDS-PAGE (Choma et al., 2000; Li et al., 2001; Zhou et al., 2000). In agreement with previous findings by others (Choma et al., 2000; Li et al., 2001; Zhou et al., 2000), we found that multiple oligomerization states, including the functional channel oligomer, coexist in the micellar preparation. Under our experimental conditions there is a population distribution of TM2 oligomers, with tetramers and pentamers being the most dominant ones.

The coexistence of multiple oligomer states of GlyR TM2 in micelles is in remarkable agreement with single-channel recording results both in authentic glycine receptors in cultured rat spinal neurons (Twyman and Macdonald, 1991) and in GlyR TM2 channels in synthetic membranes (Reddy et al., 1993). In cultured neurons, authentic GlyR exhibits four frequent conductance states, with single-channel conductance values ranging from 12 to 46 pS and the predominant ones being 27 and 46 pS (Twyman and Macdonald, 1991). In GlyR TM2 channels, the predominant conductance values are 25 and 49 pS, with 25 pS being confirmed to be from the tetrameric channels based on the same conductance value in the tethered parallel four-helix bundles (Reddy et al., 1993). High-resolution NMR data, showing only a single set of NOE connectivity, suggest either that different oligomerization states (primarily tetramers and pentamers) are in rapid exchange on the NMR time scale, yielding dynamically averaged NMR structures for the TM2 segments, or that the TM2 structures in different oligomeric states do not differ significantly from each other. In either case, the NMR structures determined in this study represent the closest approximation of the TM2 segment structure in functional channels because CD spectra in micelles and in lipid bilayers exhibit great similarity. It should be pointed out, however, that because no intersegment NOE is detected under our NOESY experimental condition (mixing time = 100 ms), the NMR data alone do not provide information about segment-segment interaction in different oligomerization states. Evaluation of possible channel architecture must therefore resort to the structural prediction by computer modeling based on NMR-derived segmental structures and the prior knowledge about the functional channel.

A plausible gating mechanism

The pentameric arrangements with the tilted and untilted TM2 helices shown in Fig. 6 could represent different states of the GlyR channel. A model of channel gating can be proposed on the basis of simultaneous tilting movement of the five TM2 segments relative to the rest of the receptor. The difference in the pore diameters for energy-minimized channel architectures with very small corresponding energy change suggests that by a mere 10° tilting of the TM2 helices the spatial packing of the helical side chains of TM2 structures, particularly those within the channel lumen, allows for transitions between the open and closed states.

Besides the side-chain hydrophilic consideration and the pore-size differences in the energy-minimized homopentameric channels, at least four additional lines of experimental evidence also support the idea of gating by entire TM2 tilting. The first is the consideration of G2′ side chain location. Position 2′ (residue 254 in α_1 and α_3, and 261 in α_2) is the only nonconserved residue in the TM2 sequences of the GlyR α isoforms, having a Gly in α_1 but an Ala in α_2 and α_3. It has been reported (Rundström et al., 1994) that replacing Gly with Ala at position 2′ results in a >10-fold decrease in GlyR sensitivity to the open channel blocker cyanotriphenylbonate (CTB) and alters the distribution of single-channel conductance states among the α isoforms, suggesting the critical involvement of G2′ in CTB binding. Moreover, because CTB binding is noncompetitive and use-dependent, channel blockage occurs only after the channel is opened. As the five TM2 segments move simultaneously from the untilted (presumably close) to the tilted (presumably open) configuration, the side chain at position 2′ is changed from the side to the center of the N-terminal entrance of the pore. When the channel is closed (as shown in Fig. 5 along the untilted lines), the G2′ side chain in the pore lumen is partially replaced by that of L3′, hindering the involvement of G2′ in CTB binding.

The second line of experimental evidence comes from the permeation and conductance measurements of various anions across the GlyR channel. It has been demonstrated (Fatima-Shad and Barry, 1993) that anions with diameters either too small or too large have low permeability and the permeability and conductance sequences for different anions are roughly inversely related. These findings suggest that ion interaction with sites within the channel plays a significant role in ion conductance. In addition, GlyR channels display anomalous mole-fraction behavior (Bormann et al., 1987; Fatima-Shad and Barry, 1993), a strong indication of multiple sites within the channel for ion interaction. Careful inspection of the channel lumen from the tilted and untilted helices (Figs. 5–7) shows that tilted helices provide at least three aligned ion-binding rings along the channel from the polar side chains of T6′, T10′, and Q14′, with possibly a fourth one at G2′. In contrast, with untilted helices, the side chains in the channel lumen are not aligned. Moreover, the large hydrophobic L3′ side chain near the intracellular entrance disrupts the continuity of the hydrophilic passage.

The third line of experimental evidence supporting our proposed gating mechanism can be found in the study of a special phenotype of hyperekplexia, which links the movement of the Q266 (Q14′) side chain to the gating of the

GlyR channel. Hyperekplexia is a disease directly related to mutations in GlyR; the only hyperekplexia mutation identified so far in the transmembrane domains is the missense mutation Q266H. This mutation greatly reduces the ability of the agonists to open the channel, yet the agonist displacement of strychnine binding is unaffected (Moorhouse et al., 1999), suggesting that the functional change of the mutation is subsequent to ligand binding. Single-channel recordings further revealed that the Q266H mutation greatly destabilizes the open channel and significantly shortens the open times. The profound change in channel gating and activation in the Q266H mutant, especially when such change occurs without associated changes in agonist binding, strongly suggests that Q266 plays an important role in the movement of the TM2 during the gating process (Moorhouse et al., 1999). In our gating model, the NMR-derived TM2 structure and the energy-minimized pore architecture show the swing of the Q266 (Q14′) side chains to narrow the pore when five TM2 segments move simultaneously from the tilted to untilted state (see the animation provided as supplementary information online). Because of the charged side chains of histidine, substituting H for Q locks the channel in the untilted state if an anion is present near the positively charged H side chain, rendering the open (tilted) channel less favorable than the closed channel in Q266H.

Whether the side chain of Q266 (Q14′) is in the channel lumen is worthy of further discussion. Based on the finding that the WT GlyR and the Q266H mutant have similar sensitivity to Zn^{2+} and pH, it has been inferred (Moorhouse et al., 1999) that although Q266 plays a crucial role in GlyR channel gating, the H266 side chain in the Q266H mutant might not be exposed to the channel lumen. This conclusion, different from ours, is derived from an implicit assumption that histidine reacts specifically with Zn^{2+} and that the effects of Zn^{2+} or proton on channel current are predominantly from actions within the pore. This appears to be the case for the homolog $GABA_A$ channel, in which H17′ (one helical turn more extracellular than Q14′) in the β_1 or β_3 subunit is thought to be part of a Zn^{2+} binding site (Horenstein and Akabas, 1998; Wooltorton et al., 1997). It should be noted that, while widely accepted for structural determination by mutagenesis, the inference about the existence of Zn^{2+} binding site is in most cases based on indirect assay of Zn^{2+} inhibition of channel current. The existence of high-affinity inhibition in the presence of histidine often suffices to suggest the histidine's involvement in Zn^{2+} binding. The lack of high-affinity inhibition, however, does not necessarily suggest that histidine is not within the pore. Given that Zn^{2+} at low concentration can potentiate glycine-activated current (Moorhouse et al., 1999), it is highly likely that the GlyR sensitivity to Zn^{2+} and H^+ results primarily from allosteric linkages rather than from direct channel blocking (Lynch et al., 1998). In short, indirect binding analysis based on inhibition of channel current can only confirm the presence of histidine in the pore when there is a high-affinity inhibition, but cannot prove the contrary in the case of no high-affinity inhibition.

The fourth line of experimental evidence in support of the idea that gating is due to entire TM2 rearrangement can be found in the mutation studies that suggest the loops of TM1-TM2 and TM2-TM3 to be the hinge points for GlyR channel gating. The most commonly observed single-point mutations in the hyperekplexia occur at R271 (Shiang et al., 1993), which borders the TM2 segment and the TM2-TM3 loop. Replacement of R271 (R19′) by an uncharged leucine or glutamine (R271L or R271Q) results in a dramatic decrease in glycine-activated currents, which is due to a decrease in the sensitivity to glycine and a redistribution of the single-channel conductance states to the lower levels. Moreover, these mutants showed no change in sensitivity to strychnine, but converted the agonists β-alanine and taurine to competitive antagonists (Rajendra et al., 1995) and the competitive antagonist picrotoxin to an allosteric potentiator and a noncompetitive antagonist (Lynch et al., 1995). Similar results are also found in other less common hyperekplexia mutations, including the recessive 1244N in the TM1-TM2 loop (Rees et al., 1994) and the dominant K276E and Y279C in the TM2-TM3 loop (Elmslie et al., 1996; Shiang et al. 1995). In the case of K276E, the functional change can only be interpreted as a consequence of impairment to the channel gating kinetics without affecting the ligand binding and channel conductance (Lewis et al., 1998). Sequential alanine substitution mutations of all residues in both loops (Lynch et al., 1997) confirmed the same results. Taken together, all mutants in the TM1-TM2 and TM2-TM3 loops seem to suggest that the loops act in parallel as hinges to allosterically couple the ligand binding to channel activation and gating. Our structural model of entire helical tilting movement for gating is consistent with the idea that the TM1-TM2 and TM2-TM3 loops are the allosteric governing points for TM2 movement.

For the neurotransmitter-gated channels in the same superfamily, two other gating models have been proposed for nACh receptor (Unwin, 1995; Wilson and Karlin, 2001). Based on the electron microscopy images at 9 Å resolution and a tentative alignment of the three-dimensional densities with the amino acid sequence, Unwin (1995) proposed that the TM2 helices of nAChR bend (or kink) near the conserved residue L9′, whose side chains form the gate of the channel. Ligand binding causes an extracellular domain rotation, which is transmitted to the level of L9′ and possibly V13′ (Unwin, 2000) to draw the hydrophobic side chains away from the central axis. This kink model, however, is not supported by the high-resolution GlyR TM2 structure determined in the present study or the recently published NMR structure of nAChR TM2 in DPC (Opella et al., 1999), which also shows TM2 to be α-helical without kinks. An alternative gating model for nAchR was proposed recently by Wilson and Karlin (Unwin, 1995; Wilson and

Karlin, 2001) who, by measuring the reaction rates of a small, sulfhydryl-specific, charged reagent with the substituted cysteines in TM1-TM2 loop and the TM2 domain and by comparing these rates for the reagent added intracellularly and extracellularly, located the gate of the closed state between αG240 (G-2′) and αT244 (T2′), and of the desensitized state between αG240 and αL251 (L9′). Although the pore radius profiles in our model showed the narrowest constriction at Q266 (Q14′), a gating location near the intracellular entrance for nAChR does not necessarily contradict our proposed model. More specifically, the charged molecular probes such as those used in the substituted cysteine accessibility measurements could likely find more constriction and slower reaction rates at levels closer to the intracellular entrance, e.g., near the level of L3′ in our closed channel model. This is because ions are believed to have to be partially (or probably fully) dehydrated before passing through the channel. Electrostatic stabilization by aligned polar groups, such as the hydroxyl groups of T6′ and T10′, as well as the amino group of Q14′ in our open channel model, can liberate ions from their hydration shells. In contrast, disruption of polar passage by bulky hydrophobic side chains, such as L3′ in our closed channel model, necessitates the ion hydration within the pore for electrostatic stability. This increases the effective radius of the ion at the level near the intracellular entrance of the closed channel. Therefore, probing with charged reagents might not necessarily reveal the true radius profile of the channel pore.

Structural consideration of channel sensitivity to anesthetics

Although structural consequences of general anesthetic effects on ligand-gated receptors may be quite complicated, our model of pore architecture built upon the NMR-derived TM2 structures offers a simple explanation as to why volatile anesthetics and short-chain alcohols can potentiate GlyR function, whereas the point mutation S267Y abolishes or even reverses such potentiation. As indicated by many recent experimental studies (Tang et al., 1997; Xu and Tang, 1997; Xu et al., 1998), anesthetic molecules are amphiphilic in nature. They favor amphipathic environments over either extremely hydrophilic or extremely hydrophobic environments and interact specifically with channel residues that are located in amphipathic interfacial regions (Tang et al., 1999a, b, 2000). The location of S267 is unique in that its polar side chain interfaces with the hydrophobic surface of M263. A recent study suggests that the second anesthetic sensitive mutation point in GlyR, A288, is in the opposite TM3 domain at the same membrane level as S267 (Mascia et al., 2000). Thus, S267 and A288, along with M263, may border an amphipathic cavity that anesthetics or short-chain alcohols can preferably occupy. Our model of channel gating involves rotational movement that relocates the Q266 side chain within the channel pore. The corresponding movement of the very next residue undoubtedly changes the shape and volume of the amphipathic cavity bordered by S267. When an amphiphilic molecule occupies and stabilizes the cavity, the dynamics of TM2 segment movement is changed. If this change is in favor of the open (tilted) state, the results will be potentiation by stabilizing and prolonging the open channel. This is apparently the case for the wild-type GlyR and $GABA_A$ receptor. If, however, anesthetic occupation of the cavity favors the closed (untilted) state, the results will be inhibition, as is probably the case for nAChR. Mutations at either S267 or A288 with different volumes of residue side chains can have similar effects. Bulky side chains can partially or completely fill the cavity to render open or closed (or even some intermediate) state more stable in the absence of anesthetics or alcohols, and thereby abolish the channel sensitivity to these neuronal agents. This view of the molecular mechanism of anesthetic action based on channel dynamics is certainly worth further investigation.

In summary, we determined the high-resolution NMR structures of TM2 segments of the human glycine receptor α_1 subunit and its anesthetic-insensitive S267Y mutant in DPC and SDS micelles. The spatial arrangements of the hydrophilic and hydrophobic side chains suggest two possible helical orientations, corresponding to an open and a closed channel upon association into a pentameric pore. A mode of channel gating is proposed based on a simultaneous 10–20° tilting rearrangement of the entire TM2 segments with respect to the rest of the receptor.

The authors thank Martha Zegarra for technical assistance and Virgil Simplaceanu, Dr. W. Milo Westler, and Dr. Chien Ho for help with use of NMR instruments, Dr. Michael Cascio for help with CD measurements. The 600-MHz NMR spectrometer was obtained through an equipment grant from the National Institutes of Health (S10 RR11248-01). The use of the National Magnetic Resonance Facility at Madison (NMRFAM) is gratefully acknowledged.

This work was supported by National Institute of General Medical Sciences Grants GM49202 (to Y.X.) and GM56257 (to P.T.), and from the Pittsburgh Supercomputing Center through NCRR (P41 RR06009) and the Commonwealth of Pennsylvania (98-125-0001).

REFERENCES

Bormann, J., O. P. Hamill, and B. Sakmann. 1987. Mechanism of anion permeation through channels gated by glycine and gamma-aminobutyric acid in mouse cultured spinal neurones. *J. Physiol.* 385:243–286.

Brejc, K., W. J. van Dijk, R. V. Klaassen, M. Schuurmans, J. van Der Oost, A. B. Smit, and T. K. Sixma. 2001. Crystal structure of an ACh-binding protein reveals the ligand-binding domain of nicotinic receptors. *Nature* 411:269–276.

Brünger, A. T. 1992. X-PLOR: A system for x-ray crystallography and NMR, Version 3.581. Yale University Press, New Heven, CT.

Choma, C., H. Gratkowski, J. D. Lear, and W. F. DeGrado. 2000. Asparagine-mediated self-association of a model transmembrane helix. *Nat. Struct. Biol.* 7:161–166.

Delaglio, F., S. Grzesiek, G. W. Vuister, G. Zhu, J. Pfeifer, and A. Bax. 1995. NMRPipe: a multidimensional spectral processing system based on UNIX pipes. *J. Biomol. NMR.* 6:277–293.

Elmslie, F. V., S. M. Hutchings, V. Spencer, A. Curtis, T. Covanis, R. M. Gardiner, and M. Rees. 1996. Analysis of GLRA1 in hereditary and sporadic hyperkeplexia: a novel mutation in a family cosegregating for hyperekplexia and spastic paraparesis. *J. Med. Genet.* 33:435–436.

Fatima-Shad, K., and P. H. Barry. 1993. Anion permeation in GABA- and glycine-gated channels of mammalian cultured hippocampal neurons. *Proc. R. Soc. Lond. B. Biol. Sci.* 253:69–75.

Franks, N. P., and W. R. Lieb. 1996. An anesthetic-sensitive superfamily of neurotransmitter-gated ion channels. *J. Clin. Anesth.* 8(3 Suppl): 3S–7S.

Garrett, D. S., R. Powers, A. M. Gronenborn, and G. M. Clore. 1991. A common sense approch to peak picking in two- and three- and four-dimensional spectra using automatic computer analysis of contour diagrams. *J. Magn. Reson.* 95:214–220.

Grenningloh, G., V. Schmieden, P. R., Schofield, P. H. Seeburg, T. Siddique, T. K. Mohandas, C. M. Becker, and H. Betz. 1990. Alpha subunit variants of the human glycine receptor: primary structures, and functional expression and chromosomal localization of the corresponding genes. *EMBO J.* 9:771–776.

Horenstein, J., and M. H. Akabas. 1998. Location of a high affinity Zn^{2+} binding site in the channel of alpha1beta1 gamma-aminobutyric acid A receptors. *Mol. Pharmacol.* 53:870–877.

Humphrey, W., A. Dalke, and K. Schulten. 1996. VMD: visual molecular dynamics. *J. Mol. Graph.* 14:27–28; 33–38.

Jorgensen, W. L., J. Chandrasekhar, J. D. Madura, R. W. Impey, and M. L. Klein. 1983. Comparison of simple potential functions for simulating liquid water. *J. Chem. Phys.* 79:926–935.

Karlin, A., and M. H. Akabas. 1998. Substituted-cysteine accessibility method. *Methods Enzymol.* 293:123–145.

Killian, J. A., T. P. Trouard, D. V. Greathouse, V. Chupin, and G. Lindblom. 1994. A general method for the preparation of mixed micelles of hydrophobic peptides and sodium dodecyl sulfate. *FEBS Lett.* 348: 161–165.

Kochendoerfer, G. G., D. Salom, J. D. Lear, R. Wilk-Orescan, S. B. Kent, and W. F. DeGrado. 1999. Total chemical synthesis of the integral membrane protein influenza A virus M2: role of its C-terminal domain in tetramer assembly. *Biochemistry* 38:11905–11913.

Kyte, J., and R. F. Doolittle. 1982. A simple method for displaying the hydropathic character of a protein. *J. Mol. Biol.* 157:105–132.

Laskowski, R. A., J. A. Rullmannn, M. W. MacArthur, R. Kaptein, and J. M. Thornton. 1996. AQUA and PROCHECK-NMR: programs for checking the quality of protein structures solved by NMR. *J. Biomol. NMR.* 8:477–486.

Lewis, T. M., L. G. Sivilotti, D. Colquhoun, R. M. Gardiner, R. Schoepfer, and M. Rees. 1998. Properties of human glycine receptors containing the hyperekplexia mutation alpha1(K276E), expressed in *Xenopus* oocytes. *J. Physiol.* 507(Pt 1):25–40.

Li, R., C. R. Babu, J. D. Lear, A. J. Wand, J. S. Bennett, and W. F. DeGrado. 2001. Oligomerization of the integrin alphaIIbbeta3: roles of the transmembrane and cytoplasmic domains. *Proc. Natl. Acad. Sci. U.S.A.* 98:12462–12467.

Luo, P., and R. L. Baldwin. 1997. Mechanism of helix induction by trifluoroethanol: a framework for extrapolating the helix-forming properties of peptides from trifluoroethanol/water mixtures back to water. *Biochemistry.* 36:8413–8421.

Lynch, J. W., P. Jacques, K. D. Pierce, and P. R. Schofield. 1998. Zinc potentiation of the glycine receptor chloride channel is mediated by allosteric pathways. *J. Neurochem.* 71:2159–2168.

Lynch, J. W., S. Rajendra, P. H. Barry, and P. R. Schofield. 1995. Mutations affecting the glycine receptor agonist transduction mechanism convert the competitive antagonist, picrotoxin, into an allosteric potentiator. *J. Biol. Chem.* 270:13799–13806.

Lynch, J. W., S. Rajendra, K. D. Pierce, C. A. Handford, P. H. Barry, and P. R. Schofield. 1997. Identification of intracellular and extracellular domains mediating signal transduction in the inhibitory glycine receptor chloride channel. *EMBO J.* 16:110–120.

MacKerell, A. D., D. Bashford, M. Bellott, R. L. Dunbrack, J. D. Evanseck, M. J. Field, S. Fischer, J. Gao, H. Guo, S. Ha, D. Joseph-McCarthy, L. Kuchnir, K. Kuczera, F. T. K. Lau, C. Mattos, S. Michnick, T. Ngo, D. T. Nguyen, B. Prodhom, W. E. Reiher, B. Roux, M. Schlenkrich, J. C. Smith, R. Stote, J. Straub, M. Watanabe, J. Wiorkiewicz-Kuczera, D. Yin, and M. Karplus. 1998. All-atom empirical potential for molecular modeling and dynamics studies of proteins. *J. Phys. Chem. B.* 102:3586–3616.

Marion, D., and K. Wuthrich. 1983. Application of phase sensitive two-dimensional correlated spectroscopy (COSY) for measurements of 1H–1H spin coupling constants in proteins. *Biochem. Biophys. Res. Commun.* 113:967–974.

Marsh, D. 1996. Peptide models for membrane channels. *Biochem. J.* 315(Pt 2):345–361.

Mascia, M. P., J. R. Trudell, and R. A. Harris. 2000. Specific binding sites for alcohols and anesthetics on ligand-gated ion channels. *Proc. Natl. Acad. Sci. U.S.A.* 97:9305–9310.

Mihic, S. J., Q. Ye, M. J. Wick, V. V. Koltchine, M. D. Krasowski, S. E. Finn, M. P. Mascia, C. F. Valenzuela, K. K. Hanson, E. P. Greenblatt, R. A. Harris, and N. L. Harrison. 1997. Sites of alcohol and volatile anaesthetic action on GABA(A) and glycine receptors [see comments]. *Nature.* 389:385–389.

Miller, C. 1989. Genetic manipulation of ion channels: a new approach to structure and mechanism. *Neuron.* 2:1195–1205.

Moorhouse, A. J., P. Jacques, P. H. Barry, and P. R. Schofield. 1999. The startle disease mutation Q266H, in the second transmembrane domain of the human glycine receptor, impairs channel gating. *Mol. Pharmacol.* 55:386–395.

Nelson, M. T., W. Humphrey, A. Gursoy, A. Dalke, L. V. Kale, R. D. Skeel, and K. Schulten. 1996. NAMD: a parallel, object oriented molecular dynamics program. *Int. J. Supercomput. Applications High Performance Computing.* 10:251–268.

Nilges, M., G. M. Clore, and A. M. Gronenborn. 1988. Determination of three-dimensional structures of proteins from interproton distance data by dynamical simulated annealing from random array of atoms. *FEBS Lett.* 239:129–136.

Opella, S. J., J. Gesell, A. R. Valente, F. M. Marassi, M. Oblatt-Montal, W. Sun, A. F. Montiel, and M. Montal. 1997. Structural studies of the pore-lining segments of neurotransmitter-gated channels. *Biochem. Mol. Biol.* 10:153–174.

Opella, S. J., F. M. Marassi, J. J. Gesell, A. P. Valente, Y. Kim, M. Oblatt-Montal, and M. Montal. 1999. Structures of the M2 channel-lining segments from nicotinic acetylcholine and NMDA receptors by NMR spectroscopy. *Nat. Struct. Biol.* 6:374–379.

Piotto, M., V. Saudek, and V. Sklenar. 1992. Gradient-tailored excitation for single-quantum NMR spectroscopy of aqueous solutions. *J. Biomol. NMR.* 2:661–665.

Polak, E. 1971. Computational Methods in Optimization. Academic Press, New York.

Rajendra, S., J. W. Lynch, K. D. Pierce, C. R. French, P. H. Barry, and P. R. Schofield. 1995. Mutation of an arginine residue in the human glycine receptor transforms beta-alanine and taurine from agonists into competitive antagonists. *Neuron.* 14:169–175.

Rajendra, S., J. W. Lynch, and P. R. Schofield. 1997. The glycine receptor. *Pharmacol. Ther.* 73:121–146.

Reddy, G. L., T. Iwamoto, J. M. Tomich, and M. Montal. 1993. Synthetic peptides and four-helix bundle proteins as model systems for the pore-forming structure of channel proteins. II. Transmembrane segment M2 of the brain glycine receptor is a plausible candidate for the pore-lining structure. *J. Biol. Chem.* 268:14608–14615.

Rees, M. I., M. Andrew, S. Jawad, and M. J. Owen. 1994. Evidence for recessive as well as dominant forms of startle disease (hyperekplexia) caused by mutations in the alpha 1 subunit of the inhibitory glycine receptor. *Hum. Mol. Genet.* 3:2175–2179.

Rundström, N., V. Schmieden, H. Betz, J. Bormann, and D. Langosch. 1994. Cyanotriphenylborate: subtype-specific blocker of glycine receptor chloride channels. *Proc. Natl. Acad. Sci. U.S.A.* 91:8950–8954.

Salom, D., B. R. Hill, J. D. Lear, and W. F. DeGrado. 2000. pH-dependent tetramerization and amantadine binding of the transmembrane helix of M2 from the influenza A virus. *Biochemistry.* 39:14160–14170.

Schlenkrich, M., J. Brickmann, A. D. MacKerell Jr., and M. Karplus. 1996. Empirical potential energy function for phospholipids: criteria for parameter optimization and applications. *In* Biological Membranes: A Molecular Perspective from Computation and Experiment. K. M. Merz and B. Roux, editors. Birkhauser, Boston. 31–81.

Scholtz, J. M., D. Barrick, E. J. York, J. M. Stewart, and R. L. Baldwin. 1995. Urea unfolding of peptide helices as a model for interpreting protein unfolding. *Proc. Natl. Acad. Sci. U.S.A.* 92:185–189.

Shiang, R., S. G. Ryan, Y. Z. Zhu, T. J. Fielder, R. J. Allen, A. Fryer, S. Yamashita, P. O'Connell, and J. J. Wasmuth. 1995. Mutational analysis of familial and sporadic hyperekplexia. *Ann. Neurol.* 38:85–91.

Shiang, R., S. G. Ryan, Y. Z. Zhu, A. F. Hahn, P. O'Connell, and J. J. Wasmuth. 1993. Mutations in the alpha 1 subunit of the inhibitory glycine receptor cause the dominant neurologic disorder, hyperekplexia. *Nat. Genet.* 5:351–358.

Smart, O. S., J. G. Neduvelil, X. Wang, B. A. Wallace, and M. S. Sansom. 1996. HOLE: a program for the analysis of the pore dimensions of ion channel structural models. *J. Mol. Graph.* 14:354–360; 376.

Tang, P., R. G. Eckenhoff, and Y. Xu. 2000. General anesthetic binding to gramicidin A: the structural requirements. *Biophys. J.* 78:1804–1809.

Tang, P., J. Hu, S. Liachenko, and Y. Xu. 1999a. Distinctly different interactions of anesthetic and nonimmobilizer with transmembrane channel peptides. *Biophys. J.* 77:739–746.

Tang, P., V. Simplaceanu, and Y. Xu. 1999b. Structural consequences of anesthetic and nonimmobilizer interaction with gramicidin A channels. *Biophys. J.* 76(5):2346–2350.

Tang, P., B. Yan, and Y. Xu. 1997. Different distribution of fluorinated anesthetics and nonanesthetics in model membrane: a 19F-NMR study. *Biophys. J.* 72:1676–1682.

Tang, P., I. Zubrzycki, and Y. Xu. 1999c. 1H-NMR spectral assignment of the second transmembrane segments of human glycine receptor. BioMagRes Bank Accession Number 4432, 4433, University of Wisconsin.

Tatulian, S. A., and L. K. Tamm. 2000. Secondary structure, orientation, oligomerization, and lipid interactions of the transmembrane domain of influenza hemagglutinin. *Biochemistry.* 39:496–507.

Tochio, H., S. Ohki, Q. Zhang, M. Li, and M. Zhang. 1998. Solution structure of a protein inhibitor of neuronal nitric oxide synthase. *Nat. Struct. Biol.* 5:965–969.

Twyman, R. E., and R. L. Macdonald. 1991. Kinetic properties of the glycine receptor main and subconductance states of mouse spinal cord neurones in culture. *J. Physiol.* 435:303–331.

Unwin, N. 1995. Acetylcholine receptor channel imaged in the open state. *Nature.* 373:37–43.

Unwin, N. 1998. The nicotinic acetylcholine receptor of the *Torpedo* electric ray. *J. Struct. Biol.* 121:181–190.

Unwin, N. 2000. The Croonian Lecture. 2000. Nicotinic acetylcholine receptor and the structural basis of fast synaptic transmission. *Philos. Trans. R. Soc. Lond. B. Biol. Sci.* 355:1813–1829.

Wilson, G., and A. Karlin. 2001. Acetylcholine receptor channel structure in the resting, open, and desensitized states probed with the substituted-cysteine-accessibility method. *Proc. Natl. Acad. Sci. U.S.A.* 98: 1241–1248.

Wooltorton, J. R., B. J. McDonald, S. J. Moss, and T. G. Smart. 1997. Identification of a Zn^{2+} binding site on the murine GABAA receptor complex: dependence on the second transmembrane domain of beta subunits. *J. Physiol.* 505(Pt. 3):633–640.

Xu, M., and M. H. Akabas. 1996. Identification of channel-lining residues in the M2 membrane-spanning segment of the GABA(A) receptor alpha1 subunit. *J. Gen. Physiol.* 107:195–205.

Xu, M., D. F. Covey, and M. H. Akabas. 1995. Interaction of picrotoxin with GABAA receptor channel-lining residues probed in cysteine mutants. *Biophys. J.* 69:1858–1867.

Xu, Y., and P. Tang. 1997. Amphiphilic sites for general anesthetic action? Evidence from ^{129}Xe-[^{1}H] intermolecular nuclear Overhauser effects. *Biochim. Biophys. Acta.* 1323:154–162.

Xu, Y., P. Tang, and S. Liachenko. 1998. Unifying characteristics of sites of anesthetic action revealed by combined use of anesthetics and nonanesthetics. *Toxicol. Lett.* 100–101:347–352.

Zhou, F. X., M. J. Cocco, W. P. Russ, A. T. Brunger, and D. M. Engelman. 2000. Interhelical hydrogen bonding drives strong interactions in membrane proteins. *Nat. Struct. Biol.* 7:154–160.

Zubrzycki, I. Z., Y. Xu, M. Madrid, and P. Tang. 2000. Molecular dynamics simulations of a fully hydrated dimyristoylphosphatidylcholine membrane in liquid-crystalline phase. *J. Chem. Phys.* 112:3437–3441.